# Time Series Forecasting Model of the Ionospheric $f_oF2$ Using Facebook Prophet

S. A. Bello[1*], N. S. Hamid[2,3], M. Abdullah[2,4], M. A. Ameen[5,6], J. S. Shehu[7], S. B. Sharafa[1], F. O. Aweda[8], K. A. Yusuf[1], S. Yahaya[1]

[1]Department of Physics, Faculty of Physical Sciences, University of Ilorin, Nigeria.
[2]Space Science Centre (ANGKASA), Institute of Climate Changes, Universiti, Kebangsaan Malaysia, Malaysia.
[3]Department of Applied Physics, Faculty of Science and Technology, Universiti Kebangsaan Malaysia, Malaysia.
[4]Department of Electrical, Electronics and Systems Engineering, Faculty of Engineering and Built, Environment, Universiti Kebangsaan Malaysia, Malaysia.
[5]Pakistan Space & Upper Atmosphere Research Commission (SUPARCO), Pakistan.
[6]Institute of Space Science & Technology (ISST), University of Karachi, Pakistan.
[7]Department of Physics, Faculty of Physical Sciences, Bayero University Kano, Nigeria.
[8]Physics Programme, College of Agriculture Engineering and Sciences, Bowen University, Nigeria.

***ABSTRACT:*** The study of ionospheric behaviour is critical for maintaining the reliability of space-based technologies, including HF communication links and Global Navigation Satellite Systems (GNSS). Ionospheric delays can significantly degrade the performance and accuracy of trans-ionospheric signals; thus, robust forecasting of the parameter is essential. This study uses a long-term dataset (2009 to 2016 for training) of observations from the Jicamarca Observatory in Peru to implement and evaluate the Facebook Prophet (FB-Prophet) time-series forecasting technique. For the years 2017 to 2019, the FB-Prophet model was used to forecast. Its performance was verified using independent observational test data and accepted empirical standards, namely the IRI-2020 URSI and CCIR sub-options. The study results indicate that FB-Prophet effectively reproduces the diurnal and semi-annual variations in the ionosphere. During the initial forecast period (2017 to 2018), FB-Prophet demonstrated superior alignment with observational fluctuations compared to empirical models, achieving a Root Mean Square Error (RMSE) of 0.71 MHz and a Mean Absolute Error (MAE) of 0.57 MHz. However, as the forecast horizon extended into the deep solar minimum of 2019, the CCIR model exhibited higher precision with a minimum RMSE of 0.15 MHz, while FB-Prophet's uncertainty interval expanded as the lead time increased, and the solar environment transitioned into a significantly quieter regime. These findings demonstrate that FB-Prophet's time-series decomposition is a highly effective tool for multi-year ionospheric forecasting at equatorial latitudes. The study highlights that while empirical models remain reliable for long-term climatological averages, the FB-Prophet approach offers enhanced predictive accuracy for capturing non-linear variations during periods of moderate solar activity (107.68 ± 33.81 sfu).

***KEYWORDS:*** Ionosphere, Critical frequency, Facebook Prophet, $f_oF2$ , Time series forecasting.

[Received Jan. 01, 2026; Revised Mar. 19, 2026; Accepted Mar. 24, 2026] Print ISSN: 0189-9546 | Online ISSN: 2437-2110

## I INTRODUCTION

Situated within the Earth's atmosphere, the ionosphere is characterized by the presence of partially ionized gases that form an interface between the atmosphere and space (Kelley, 2009). The trans-ionospheric signals can be affected by the prevailing conditions of the ionosphere. Applications such as Global Navigation Systems of Satellite (GNSS) and high-frequency (HF) dependent systems' radio signals can be altered by the ionosphere. The ionosphere is stratified into several layers depending on the time of the day. The critical (or maximum) frequency of the ionospheric F2-layer ($f_oF2$) is considered a major parameter of the ionosphere. It has a direct relationship with the electron density of the ionosphere (i.e., $mF2 = 1.24 \times (f_oF2)^2 \times 10^{10}\ m^3$ ). The values of $f_oF2$ can vary due to the concentration of photoionization owing to the intensity of the sun, solar cycle and extreme space weather events like solar flare bursts, coronal mass ejections (CME), solar winds, etc. The variability of the ionosphere can be greatly impacted due to different severe space weather events, thereby affecting the affecting the reliability of the communication and navigation system (Basu et al., 2002). At the equatorial ionosphere, ionosphere, even during the

*Corresponding author: *bello.sa@unilorin.edu.ng*
*doi:* http://doi.org/10.63746/njtd.v23i1.4395

geomagnetic quiet period, the behaviour of the ionosphere is complex due to the ionospheric F-region dynamo and the near horizontal geomagnetic field lines configuration responsible or the plasma transport (Acharya et al., 2012; Bi et al., 2022). The plasma transportation processes in the equatorial ionospheric F-layer comprise the vertical plasma drift and diffusion of plasma away to the higher latitudes. The described phenomenon is referred to as the equatorial ionospheric anomaly (EIA), which is characterized by a trough in ionization at the magnetic equator and crests at low latitudes.

Studying the morphology along with the behaviour of the ionosphere under certain conditions is crucial to satellite communication systems, which include navigation, remote sensing, and security. This is the reason aeronomy scientists are focused on studying the characteristics and behaviour of the ionosphere, mechanisms, and dynamics and the necessary physics and empirical base models for the prediction of the ionosphere (Akala et al., 2010). This, in turn, has impacted the various forecasting modelling approaches of the ionosphere. The forecasting model techniques involve the prediction of time-series data values ahead of time over a certain horizon. In the context of forecasting techniques, the horizon is defined as the number of periods in the future that is to be forecasted.

Several forecasting model techniques are useful for predicting future trends, and examples of such models are the entropy weight method (Bai et al., 2020), the autoregressive algorithm (Tsagouri et al., 2009), artificial neural networks (Athieno et al., 2017), regressive models (Liu et al., 2003), the Facebook Prophet (FB-prophet) model (Elseidi, 2024; Toharudin et al., 2023), etc. The FB-prophet model used in this study is an open-source forecasting modelling tool developed by Facebook in 2017 (Vishwas & Patel, 2020). Currently, the FB- Prophet model package is available in Python and R languages.

In recent times, the model has been applied in the field of atmospheric physics. For example, Oo and Sabai (2020) used the FB-prophet model to forecast the temperature of Myitkyina city in Myanmar. Their results show that the FB-prophet model gave a good prediction of temperature over the study region and is found useful as an alternative to other meteorological techniques. Similarly, Toharudin et al. (2023) used long short-term memory (LSTM) and FB-prophet to forecast the diurnal variations of air temperature over Bandung. Their result shows that the difference in the RMSE values of both models is not significant. The model performance of the FB-prophet of the air temperature peak value is better than that of the compared LSTM model.

The FB-Prophet model has been effectively expanded to ionospheric research outside of meteorological applications in recent years. For example, Tang et al. (2022) applied the model to global ionospheric TEC forecasting by predicting 15th-order spherical harmonic coefficients, concluding that a 15-day historical training period provided optimal performance with Root Mean Square Error (RMSE) values ranging from 1.1 to 3.4 TECU depending on solar activity levels. Similarly, Huang et al. (2022) integrated the NeuralProphet hybrid framework with multiple factors, including solar and geomagnetic indices, to construct a regional TEC forecasting model (MF-NPM). Their findings indicated that this multi-factor approach achieved a relative accuracy of over 93% and significantly outperformed standard long short-term memory (LSTM) networks during both solar maximum phases and geomagnetic storms. By building upon these successful TEC applications, the present study implements FB-Prophet to evaluate its efficacy in forecasting the critical frequency $f_oF2$ at an equatorial station.

While empirical models such as the International Reference Ionosphere (IRI) remain the standard for climatological representation (Bilitza et al., 2017), they often struggle to capture the short-term variability and non-linear responses of the $f_oF_2$ parameter, particularly at equatorial latitudes like Jicamarca (Bello et al., 2023). Although modern Machine Learning (ML) techniques, such as Long Short-Term Memory (LSTM) networks and Artificial Neural Networks (ANN), have improved predictive accuracy in recent years (Tang et al., 2022), these models often function as 'black boxes'. Their high computational overhead and lack of physical interpretability make it difficult to isolate how the model handles the ionosphere's complex, multi-scale periodicities.

In contrast, the Facebook Prophet (FB-Prophet) model offers a distinct advantage by utilizing an additive regression framework that explicitly decomposes the time series into trend, multi-period seasonality, and disturbance effects (Taylor & Letham, 2018). This study specifically tests FB-Prophet for $f_oF_2$ forecasting because its 'decomposable' nature allows for the simultaneous modelling of diurnal and semi-annual oscillations (Toharudin et al., 2023). Furthermore, the model remains robust to the missing data points and outliers often encountered in digisonde observations, a significant limitation for many deep learning architectures. By addressing the rigidity of empirical models and the complexity of deep learning, this research aims to establish whether a trend-seasonality decomposition approach can provide a more efficient and interpretable forecast for equatorial ionospheric dynamics.

The present study used the ionospheric $f_oF2$ digisonde sounder measurements at an equatorial station. Using the FB-prophet package on Python called Prophet, the $f_oF2$ model was developed and compared with the observational measurement.

## II MATERIALS AND METHOD

### A. Ionospheric Data and Processing

This study utilizes the ionospheric critical frequency ($f_oF2$) obtained from a Digital Portable Sounder (DPS) digisonde machine located at the Jicamarca station (12° S, 76.9° W, dip latitude: 1.0° N). The sounding interval is 15 minutes, with data products archived by the Global Ionospheric Radio Observatory (GIRO) Reinisch & Galkin (2011), and the numerically scaled $f_oF2$ values are available for download from https://giro.uml.edu/didbase/scaled.php. To ensure the integrity of the analysis, data quality control was enforced by filtering observations based on the Confidence Score (CS) (Galkin et al., 2013; Reinisch et al., 2005), a method commonly employed in other research studies (Bello et al., 2017a; Bello et al., 2017b; Bello et al., 2017c; Bello et al., 2019; Bello et al., 2023). This processing, including data

cleaning and CS filtration, was executed using the DinData software (Bello et al., 2025) developed at the University of Ilorin, Nigeria and can be downloaded from https://doi.org/10.5281/zenodo.17937258. Following filtration, the 15-minute observations were averaged hourly and resampled to provide daily values. The analysis period spans thirteen years, from 2009 to 2021, covering both the solar minimum and maximum conditions of Solar Cycle 24 and the transition into Solar Cycle 25.

B. Solar Activity Modelling

To observe the influence of solar activity on $f_oF2$, the $F_{10.7}$ solar radio flux was analyzed. The training phase of the $f_oF2$ (2009 to 2016) has a mean flux of $107.68 \pm 33.81$ sfu, while the testing phase of $f_oF2$ (2017 to 2019) reflected a quieter solar environment with a mean flux of $74.45 \pm 9.28$ sfu. The $F_{10.7}$ solar radio flux data (local noon-time observed $F_{10.7}$ values in s.f.u., $(10^{-22}\, Wm^{-2}Hz^{-1})$ are provided by the Dominion Radio Astrophysical Observatory and Natural Resources Canada, as described in (Tapping, 2013) and are available for download at https://kp.gfz.de/app/files/Kp_ap_Ap_SN_F107_since_1932.txt. The observed solar activity during the study period is classified according to Wang et al. (2017), where $F_{10.7}$ values up to 100 sfu denote low activity, while values ranging from 100 to 150 sfu represent moderate solar activity.

To extrapolate solar flux trends through 2030, an empirical model was fitted using a four-parameter Gaussian function to represent cycle morphology:

$$F(t) = a \cdot \exp\left(-\frac{(t-b)^2}{2c^2}\right) + d \quad (1)$$

In this expression, $t$ denotes time in years since 1 January 2020. The parameters $a$ (amplitude), $b$ (peak timing), $c$ (cycle width), and $d$ (baseline flux) were derived using nonlinear least-squares regression with bisquare weighting to minimize the influence of transient outliers.

C. FB-Prophet Modelling

The Facebook Prophet model is a decomposable time series framework that models the observed $f_oF2$ as a summation of trend, seasonality, and residual components (Harvey & Peters, 1990):

$$y(t) = g(t) + s(t) + \epsilon_t \quad (2)$$

The trend component $g(t)$ is implemented via a piecewise linear model defined as:

$$g(t) = (k + a(t)^T\delta)t + (m + a(t)^T\gamma) \quad (3)$$

where $k$ is the base growth rate, $\delta$ represents trend change adjustments, and $m$ is the offset. The seasonality component $s(t)$ employs a Fourier series:

$$s(t) = \sum_{n=1}^{N}\left(a_n \cos\left(\frac{2\pi n}{P}\right) + b_n \sin\left(\frac{2\pi n}{P}\right)\right) \quad (4)$$

where $P$ is the defined model period.

FB-prophet typically uses time $(t)$ as its regressor and works by fitting many linear and nonlinear functions of time as components (Toharudin et al., 2023). The FB-prophet model is flexible and allows the forecaster to customize the model's functional components. As in the case of this study, the holiday effect is excluded from the model configuration. The data used are mainly periods that are considered geomagnetically quiet days.

The systematic workflow adopted in this study is illustrated in Figure 1. The process begins with the acquisition of raw ionospheric $f_oF2$ data from the GIRO database, which undergoes rigorous quality control using the DinData software and confidence score (CS) filtration. Following this, the solar activity baseline is established through a four-parameter Gaussian model of the $F_{10.7}$ flux. These processed data streams serve as the foundation for the FB-Prophet time-series model, which utilizes piecewise linear trends and Fourier-based seasonality to generate long-term ionospheric forecasts. Finally, the predictive performance of the FB-Prophet framework is quantitatively assessed and compared against standard climatological IRI-2020 models to determine its effectiveness in capturing ionospheric variability during various solar activity phases.

To ensure the reliability of the training dataset, raw ionospheric measurements were processed using the DinData software. Only data points with an associated CS $\geq 70$ (Bello et al., 2017a; Bello et al., 2017b; Bello et al., 2017c; Bello et al., 2019; Bello et al., 2023) were utilized, effectively removing low-quality observations. No data imputation techniques were applied to fill gaps within the dataset; rather, the FB-Prophet model was calibrated to process the intermittent temporal structure of the filtered data directly. This methodology prioritizes the integrity of the observational inputs over continuous data completion, ensuring that the model parameters are constrained solely by high-confidence measurements.

To establish a robust empirical baseline for evaluating the FB-Prophet framework, hourly values were obtained using the International Reference Ionosphere (IRI) model. Specifically, the IRI-2020 FORTRAN codes were implemented to generate predictions via the International Union of Radio Science (URSI) and the Consultative Committee on International Radio (CCIR) sub-options. These IRI models serve as recognized empirical standards (ISO 16457:2022, https://www.iso.org/standard/79476.html) for long-term climatological averages, providing a rigid comparison against which the predictive accuracy and non-linear capturing capabilities of the FB-Prophet model were quantitatively verified. The IRI model's history, current state, and recent advancements are all covered in a recent review study by Bilitza et al. (2022).

D. Model Configuration and Evaluation

The FB-Prophet model was configured with a linear growth trend and additive seasonality, incorporating both yearly and weekly periodicities. Table 1 summarizes the final hyperparameter settings utilized for the model configuration. Holiday effects were excluded from the analysis.

**Table 1** FB-Prophet Final Hyperparameter Settings

| Hyperparameter | Value | Description |
|---|---|---|
| Growth Model | Linear | Standard piecewise linear trend |
| Seasonality Mode | Additive | Constant seasonal impact |
| Changepoint Prior Scale | 0.05 | Controls trend flexibility |
| Seasonality Prior Scale | 10.0 | Controls seasonal strength |
| Yearly/Weekly Seasonality | Enabled | Fourier series components |

To ensure the FB-Prophet model was optimized for the equatorial ionospheric characteristics of Jicamarca, a hyperparameter tuning process was conducted. The initial training dataset (2009 to 2017) was divided into a sub-training set (2009 to 2014) and a validation set (2015 to 2017). This validation slice was used to evaluate the model's sensitivity to key hyperparameters, specifically the Changepoint Prior Scale and Seasonality Prior Scale.

Through a grid search approach, the Changepoint Prior Scale was tested across a range of 0.001 to 0.5. A value of 0.05 was selected as it provided the optimal balance between capturing legitimate ionospheric trend shifts (e.g., solar cycle transitions) and avoiding over-fitting to short-term noise. Similarly, the Seasonality Prior Scale was set to 10.0 after validation showed that higher values allowed the model to more accurately reflect the strong diurnal and semi-annual oscillations characteristic of the equatorial $f_oF_2$. The final parameters (summarized in Table 1) were then fixed before the model was applied to the independent test environment (2017 to 2019).

Model performance was assessed by comparing the predicted values against the observed $f_oF2$ data using the Mean Absolute Error (MAE):

$$MAE = \frac{1}{N}\sum_{i=1}^{N}|y_i - \hat{y}_i| \tag{5}$$

and Root Mean Square Error (RMSE):

$$\text{RMSE} = \sqrt{\frac{1}{N}\sum_{i=1}^{N}(y_i - \hat{y}_i)^2} \tag{6}$$

where $N$ is the number of observations, $y_i$ is the observed measurement, and $\hat{y}_i$ is the predicted $f_oF2$ values.

In addition to standard error metrics, a residual analysis was performed to evaluate the model's sensitivity to solar forcing. The prediction residuals, denoted as $\Delta f_oF_2$, represent the point-by-point difference between the observed and predicted values, defined as:

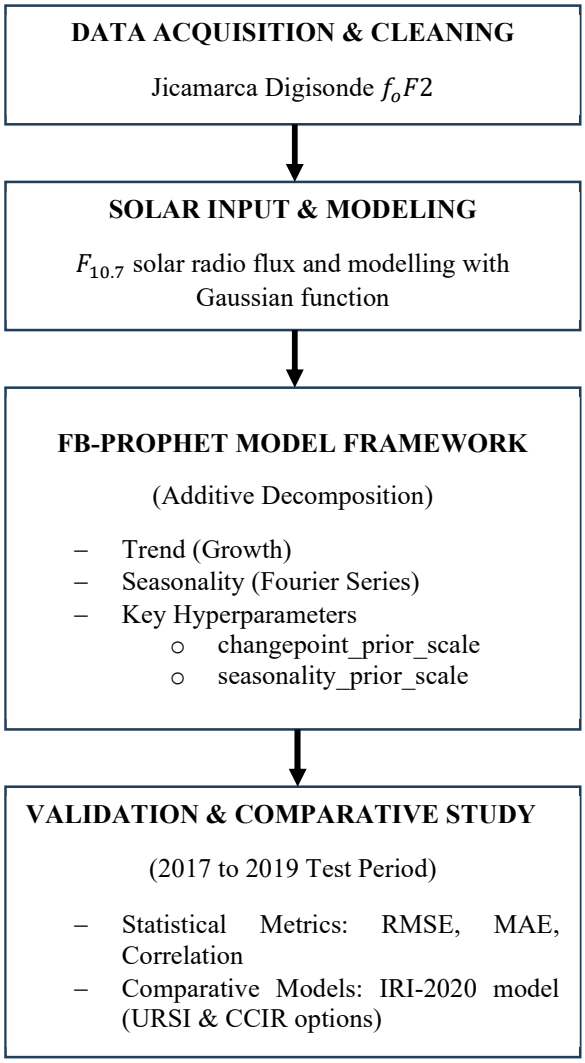


**Figure 1** A block diagram illustrating the methodology used in the study.

The diagram outlines the workflow from data acquisition and cleaning using DinData to the integration of solar activity indices and the FB-Prophet time-series forecasting framework. The process culminates in a comparative validation against established IRI (URSI and CCIR) models using standardized error metrics (RMSE and MAE).

$$\Delta f_oF_2 = f_oF2_{obs} - f_oF2_{FB} \tag{7}$$

where $f_oF2_{obs}$ is the observational data from the Jicamarca digisonde and $f_oF2_{FB}$ is the value predicted by the FB-Prophet model.

To determine if the model error is systemically driven by solar activity levels, these residuals were correlated with the $F_{10.7}$ solar index using the Pearson correlation coefficient ($r$), calculated as:

$$r = \frac{\sum_{i=1}^{n}(\Delta f_oF_2(i) - \overline{\Delta f_oF_2})(F_{10.7}(i) - \overline{F_{10.7}})}{\sqrt{\sum_{i=1}^{n}(\Delta f_oF_2(i) - \overline{\Delta f_oF_2})^2 \sum_{i=1}^{n}(F_{10.7}(i) - \overline{F_{10.7}})^2}} \tag{8}$$

where $n$ is the number of daily observations in the test period, and the overbars denote the arithmetic means of the respective variables. This quantitative approach allows for a rigorous

assessment of whether the model's predictive uncertainty is a linear function of solar flux intensity.

## III RESULTS AND DISCUSSION

The temporal progression of the $F_{10.7}$ flux, illustrated in Figure 2, demonstrates the transition between Solar Cycle 24 and the ongoing peak phase of Cycle 25. The model's predictive accuracy is validated across the three distinct phases: the training interval, which captured the peak activity of Cycle 24; the testing interval (2017 to 2019), characterized by a quieter solar environment with a mean flux of 74.45 $\pm$ 9.28 sfu; and the recent 2020 to 2026 period, which reflects the rapid rise toward the current solar maximum.

The four-parameter Gaussian model provides a robust empirical visualization of the Solar Cycle 25 morphology. By utilizing the training and testing datasets to constrain the baseline $(d)$ and amplitude $(a)$, the model projects a characteristic cycle peak that aligns with the observed recent activity in 2024 to 2025. The inclusion of the 2020 to 2026 observational data confirms that the Gaussian fit captures the trajectory of Cycle 25 with high fidelity, serving as a reliable baseline for interpreting the ionospheric $f_oF2$ variations modelled via the FB-Prophet framework. Despite the inherent symmetry of the Gaussian function, its alignment with the recent observational data (green) validates its utility as a physically plausible tool for long-term solar activity visualization.

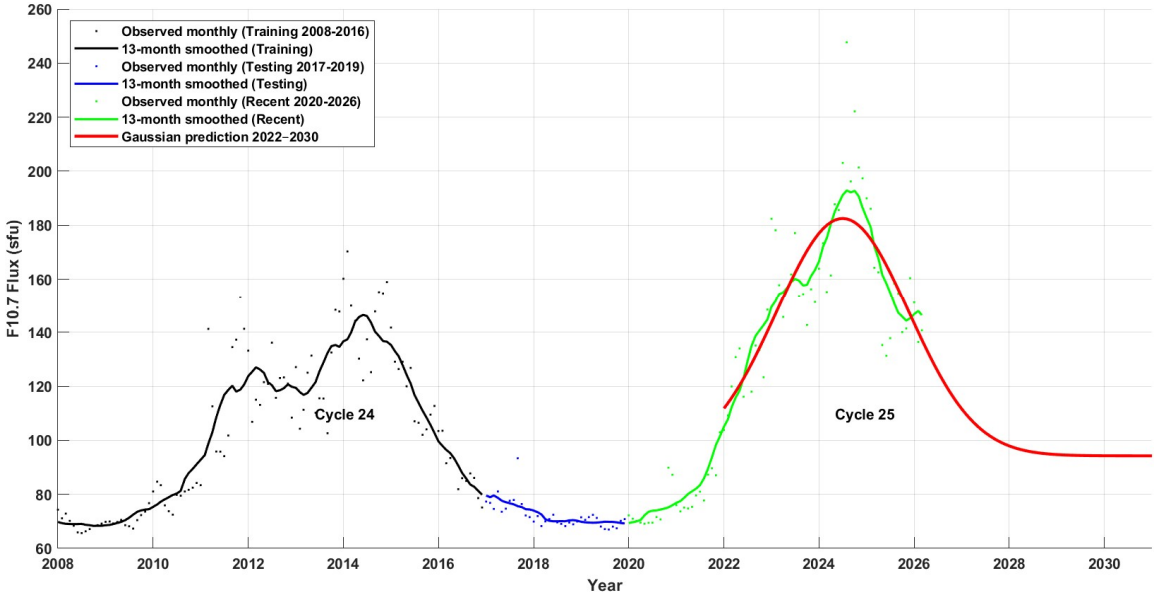


**Figure 2** Multi-phase temporal evolution and Gaussian prediction of the $F_{10.7}$ solar flux (2008 to 2030). Observed monthly data are stratified into three distinct intervals: training (2008 to 2016, black), testing (2017 to 2019, blue), and the most recent observational period (2020 to 2026, green). Corresponding 13-month centered moving averages are plotted for each phase. The empirical projection for Solar Cycle 25 (red line) is derived from a four-parameter Gaussian model, providing a visualization of the cycle morphology through 2030.

The hourly and daily variations of ionospheric $f_oF2$ parameters are shown in Figure 3. The values of $f_oF2$ exhibit diurnal and annual variation. The semi-annual variation can also be observed, indicating the occurrence of seasonality in the $f_oF2$ parameter. The effect of solar activity influences the variation in the $f_oF2$ values. The value of $f_oF2$ increased from a daily peak value of 7.56 MHz in 2009 to 11.57 MHz in 2014. Typically, both the hourly (grey points) and the daily (blue points) are higher during the solar maximum conditions of solar cycle 24 (between the years 2011 and 2015). The observational dataset of $f_oF2$ from 2009 to 2021 is divided into three portions. The FB-prophet model is trained using the daily $f_oF2$ data from 2009 to 2016. The model is tested against observational $f_oF2$ within the years 2017 to 2019.

The FB-prophet model output of $f_oF2$ is illustrated in Figures 4 and 5, showing the model predictions, trends and yearly seasonal variations. In Figure 4, the $f_oF2$ observational data that contributed to the model's training are shown by the black dotted points. The model's resulting prediction is displayed by the blue lines, which include the 95% upper and lower confidence intervals.

The FB model effectively reconstructed the $f_oF2$ variations during the observational gap from 2012 to 2013. While direct validation is precluded by the lack of ground-truth data, the model demonstrates high climatological fidelity by accurately capturing the solar-cycle-driven rise in $f_oF2$ as solar activity intensified toward the peak of Solar Cycle 24 (Figure 5a). Similarly, the model correctly describes the semi-annual

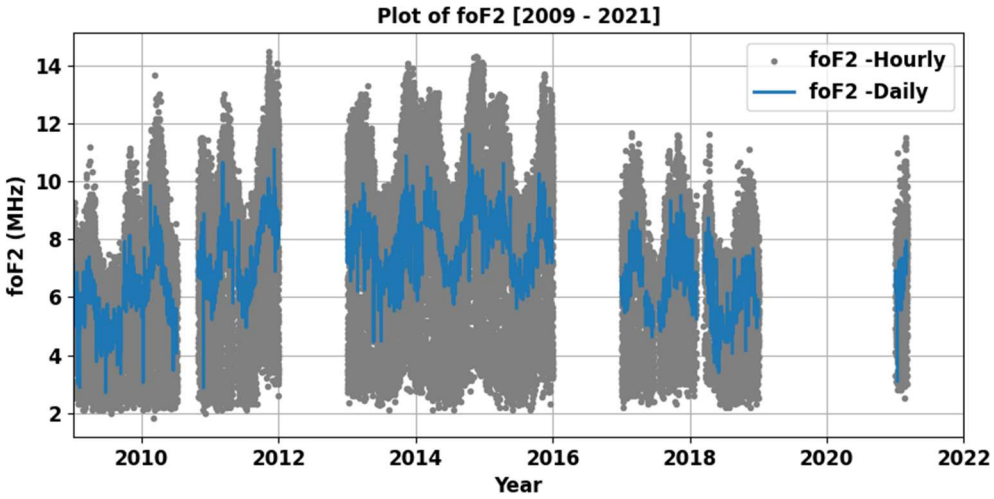


**Figure 3** The variation of the ionospheric $f_oF2$ profile parameter for the years between 2009 and 2021. The grey points indicate the hourly values, while the blue line indicates the daily averages.

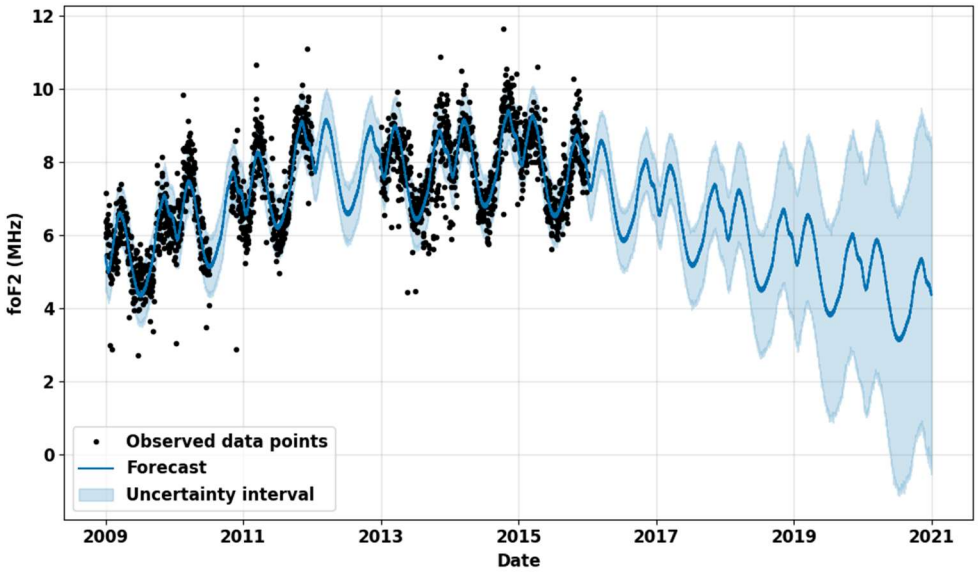


**Figure 4** The FB-prophet model prediction of the daily values of ionospheric $f_oF2$ .

variations in $f_oF2$ by identifying two annual peaks that represent the March and September equinoxes (Figure 5b).

Figure 6 illustrates the $f_oF2$ forecast generated by the FB-Prophet model over a 4-years horizon (2017 to 2019), alongside the URSI and CCIR sub-options of the International Reference Ionosphere (IRI). The observational data (orange dashed line), sourced from the Jicamarca station, represents an independent test set not utilized during the model training phase. The corresponding statistical performance of these models, quantified by Mean Absolute Error (MAE) and Root Mean Squared Error (RMSE), is presented in Figure 7. During the initial forecast period (2017 to 2018), FB-Prophet demonstrated superior alignment with observational fluctuations, achieving an RMSE of 0.71 MHz and an MAE of 0.57 MHz, which outperformed the CCIR model's RMSE of 0.80 MHz during the same period.

As shown in Figure 7, FB-Prophet achieved an RMSE of 0.71 MHz and an MAE of 0.57 MHz in 2017. During this same period, the CCIR model exhibited the highest deviation with an RMSE of 0.80 MHz, suggesting that the time-series decomposition approach of FB-Prophet is more effective at capturing ionospheric variability during moderate solar activity than standard empirical maps. All three models successfully capture the fundamental seasonal oscillations and the progressive decline in $f_oF2$ values as the solar cycle transitioned toward the minimum of Solar Cycle 24. By 2019, the error metrics for all models decreased significantly. Notably, the CCIR model outperformed the other options during the deep solar minimum, reaching a minimum RMSE of 0.15 MHz compared to FB-Prophet's 0.43 MHz (Figure 7). As the forecast horizon extends beyond 2018, the uncertainty interval (shaded region in Figure 6) of the FB-Prophet model expands. This non-uniform expansion during the transition into the deep solar minimum occurs because the model, which was trained on a high-variance solar regime ($107.68 \pm 33.81$ sfu), encountered a significantly quieter and more stable environment ($74.45 \pm 9.28$ sfu) that sits at the edge of its

primary training variance, leading to a natural decrease in predictive confidence. This indicates that while the model effectively reproduces periodic variations based on historical trends, predictive confidence diminishes as the lead time increases. In contrast, the URSI and CCIR models maintain a rigid empirical path based on long-term climatological averages.

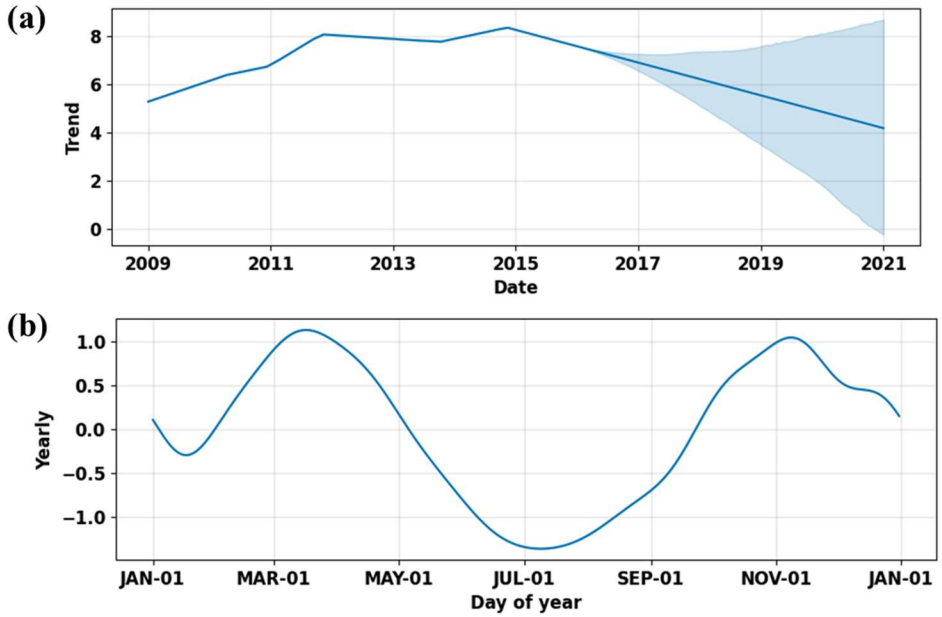


Figure 5: FB-prophet model diagnostic plot showing (a) Trend (b) yearly variations in $f_oF2$

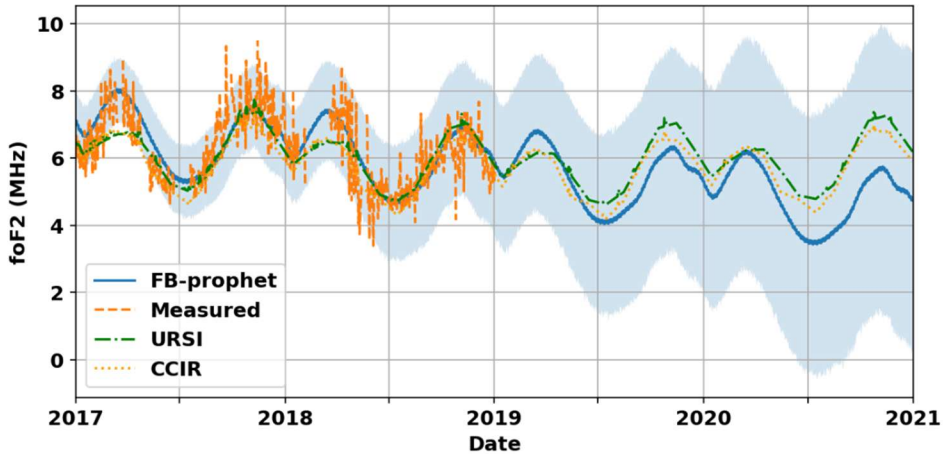


**Figure 6** Comparison of observational $f_oF2$ values from the Jicamarca station (2017 to 2019) with the FB-Prophet model and the IRI-2020 model options (URSI and CCIR). The shaded area indicates the uncertainty interval for the FB-Prophet forecast as it extends toward 2021

The disparity in model performance during the 2019 deep solar minimum (see Figure 1) highlights the contrasting nature of empirical and statistical modelling. The CCIR model achieved a minimum RMSE of 0.15 MHz because of the stable solar environment ($74.45 \pm 9.28$ sfu) aligned perfectly with the long-term climatological averages upon which the model is based. Conversely, FB-Prophet's error of 0.43 MHz reflects the challenge of statistical extrapolation. Having been trained on more dynamic and higher-flux data ($107.68 \pm 33.81$ sfu), the model encountered a regime shift in 2019 that led to an expansion of its uncertainty interval. While FB-Prophet is more effective at capturing high-frequency non-linearities during active periods, empirical models like CCIR remain superior for predicting the stable, low-variance conditions characteristic of a deep solar minimum.

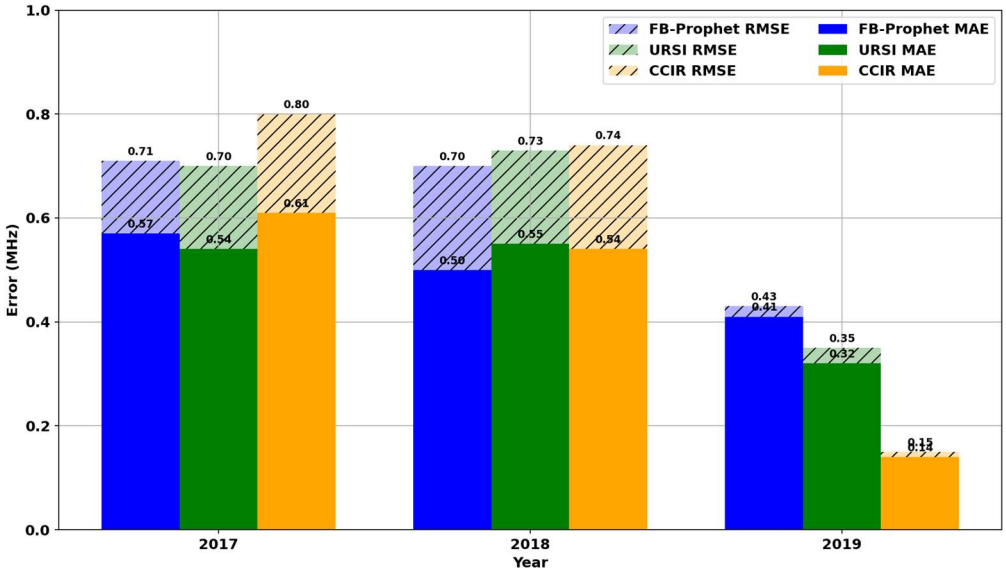


**Figure 7** Comparison of prediction errors for FB-Prophet, URSI, and CCIR models over the period 2017 to 2019. The solid bars represent the Mean Absolute Error (MAE), while the hatched regions indicate the Root Mean Squared Error (RMSE) in MHz.

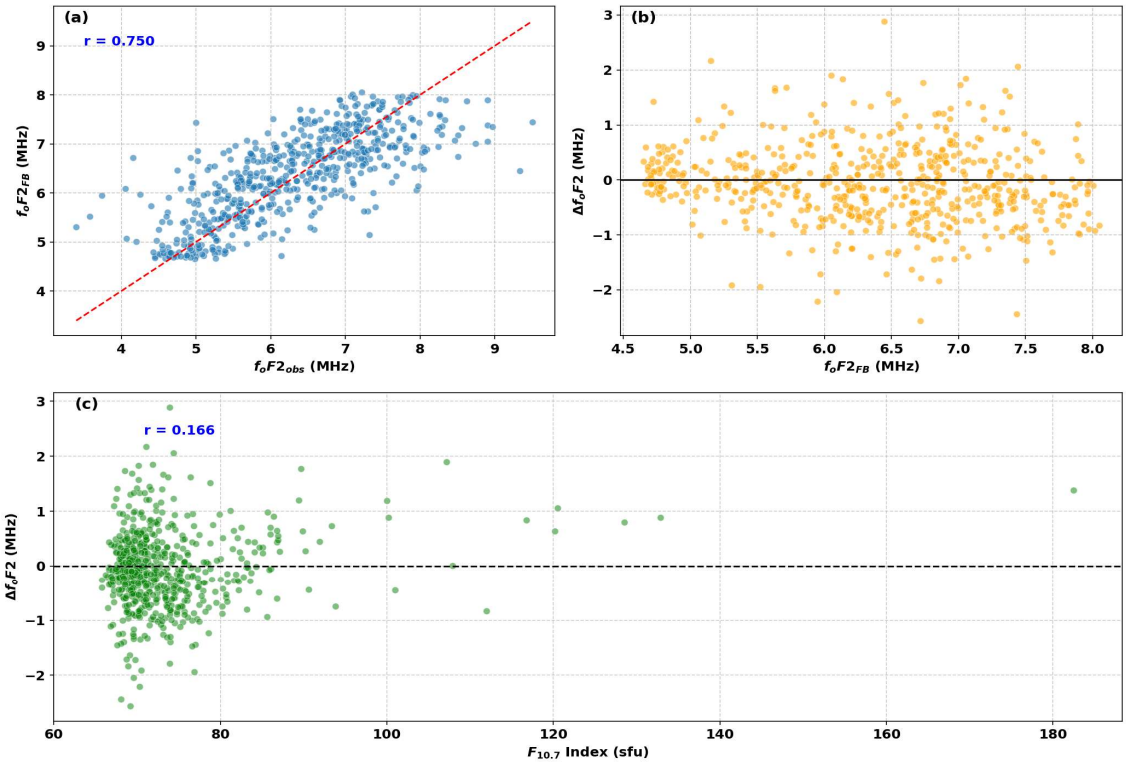


**Figure 8** Statistical diagnostic of the FB-Prophet model performance for $f_oF2$ forecasting at Jicamarca (2017 to 2019). (a) Scatter plot of observed vs. predicted $f_oF2$ values showing the 1:1 reference line and Pearson correlation coefficient ($r$). (b) Residual plot showing the distribution of prediction errors ($\Delta f_oF_2$) against predicted values to assess model bias. (c) Correlation analysis of prediction residuals against the $F_{10.7}$ solar index, illustrating the model's stability across varying levels of solar activity.

The statistical performance of the FB-Prophet model is quantitatively summarized in the diagnostic plots of Figure 8. The scatter plot in Figure 8(a) reveals a strong linear relationship between the observed and predicted $f_oF_2$, with a Pearson correlation coefficient of $r = 0.750$. This indicates that the model successfully captures approximately 75% of the variance in the equatorial ionosphere at Jicamarca, effectively tracking both diurnal and seasonal cycles during the 2017 to 2019 test period.

The residual analysis in Figure 8(b) shows a balanced distribution of errors around the zero-mean line, suggesting the absence of significant systemic bias. Furthermore, to

address the influence of solar forcing on model error, Figure 8(c) displays the residuals against the $F_{10.7}$ solar index. The resulting correlation of $r = 0.166$ demonstrates a very weak dependency between prediction errors and solar activity. This quantitative result confirms that the expansion of the uncertainty interval during the solar minimum is not a linear consequence of declining solar flux but is instead attributed to the increased relative impact of stochastic background noise when solar driving forces are at their lowest.

The robust performance of FB-Prophet during the 2017 to 2019 period is consistent with recent applications of the model in ionospheric TEC forecasting. For instance, Tang et al. (2022) demonstrated that Prophet-based models can achieve high accuracy (RMSE 1.1 to 3.4 TECU) by capturing periodic fluctuations that empirical products often miss. Similarly, the findings of Huang et al. (2022), which showed Prophet-based models achieving over 93% accuracy even during disturbed solar conditions, supports our observation that time-series decomposition provides a superior alignment with observational fluctuations compared to the rigid paths of IRI-2012 sub-options. Furthermore, the expansion of uncertainty observed in our results during the solar minimum mirrors the limitations noted by Tang et al. (2022), where statistical extrapolation becomes less precise when the target environment lacks the dynamic cyclicality present in the training data.

Kouris and Nissopoulos (1994) performed a comparison of $f_oF2$'s dependence on six separate indices, which included the SSN (sunspot number), $F_{10.7}$, IF2 (the ionospheric index of solar activity), the index IG, the Australian index, and the Russian ionospheric index. The findings from their analysis of $f_oF2$'s variability with these indices demonstrate that the F2-layer's maximum frequency exhibits a direct proportionality with the magnitude of the ionizing radiation. Another study by Adebesin et al. (2014) compared the annual variation of $f_oF2$ over three solar epochs. They found that $f_oF2$ values are consistently higher during high solar activity than the values recorded during both moderate and low solar activity conditions. From Figure 6, the FB-Prophet forecast between 2017 and 2019 showed the influence of the $F_{10.7}$ solar cycle in the model predictions as expected.

## IV. CONCLUSION

This study evaluated the long-term dynamics of ionospheric $foF2$ at the equatorial Jicamarca station by implementing the FB-Prophet time-series model. By utilizing additive components to decompose trend and seasonality, the model successfully reproduced characteristic variations over a five-year long-term extrapolation horizon, identifying semi-annual peaks during equinoctial seasons. Quantitative analysis demonstrates that FB-Prophet provides a robust forecasting capability, particularly during the initial 1 to 2 years (2017 to 2018), where it achieved a Root Mean Square Error (RMSE) of 0.71 MHz and outperformed the IRI-2020 sub-options in capturing high-frequency fluctuations. These findings suggest that while empirical models remain the standard for long-term climatological averages, the FB-Prophet approach offers a valuable complementary tool for multi-year ionospheric forecasting, particularly for enhancing predictive accuracy during the first half of the forecast horizon at equatorial latitudes. However, as the forecast horizon extended into the deep solar minimum of 2019 to 2021, the model's uncertainty interval expanded significantly, reflecting a diminished predictive confidence inherent in long-term statistical extrapolation. During this phase, the empirical CCIR model demonstrated superior precision with a minimum RMSE of 0.15 MHz. It is important to note that FB-Prophet is a statistical decomposition tool that captures non-linear variations by fitting mathematical functions to historical trends; it does not account for the underlying physical mechanisms or plasma dynamics of the ionosphere.

## AUTHOR CONTRIBUTIONS

S. A. Bello conceptualized the study, developed the methodology and software, performed validation and investigation, handled data curation, and wrote the original draft; N. S. Hamid provided supervision and formal analysis and contributed to reviewing and editing the manuscript; M. Abdullah provided supervision and contributed to the review and editing process; M. A. Ameen wrote the IRI-2020 FORTRAN code and the review of the manuscript; J. S. Shehu contributed to methodology development, validation, and manuscript editing; S. B. Sharaf assisted with formal analysis, visualization, and editing of the manuscript; F. O. Aweda assisted with literature review and the final review of the manuscript; K. A. Yusuf contributed to data curation, validation, and the final review of the manuscript; S. Yahaya assisted with literature review and manuscript editing.

## ACKNOWLDGEMENT

The authors thank the staff at Jicamarca Radio Observatory and the Lowell Global Ionosphere Radio Observatory (GIRO) Data Centre (http://giro.uml.edu/) for making the $f_oF2$ data available. The $F_{10.7}$ solar indices plots were acquired from Dominion Radio Astrophysical Observatory and Natural Resources Canada. The authors also express their gratitude to the anonymous reviewers for their insightful comments and suggestions, which significantly improved the quality and clarity of this manuscript.

## REFERENCES

**Acharya, R., Roy, B., Sivaraman, M., & Dasgupta, A. (2012).** Improved predictions of equatorial TEC for real time applications. *Advances in Space Research, 49*(4), 694-699. https://doi.org/10.1016/j.asr.2011.11.006

**Adebesin, B., Adekoya, B., Ikubanni, S., Adebiyi, S., Adebesin, O., Joshua, B., & Olonade, K. (2014).** Ionospheric foF2 morphology and response of F2 layer height over Jicamarca during different solar epochs and comparison with IRI-2012 model. *Journal of Earth System Science, 123*(4), 751-765. https://doi.org/10.1007/s12040-014-0435-y

**Akala, A., Adeloye, A., & Somoye, E. (2010)**. Ionospheric foF2 variability over the Southeast Asian sector. *Journal of Geophysical Research: Space Physics, 115*(A9). https://doi.org/10.1029/2010JA015250

**Athieno, R., Jayachandran, P., & Themens, D. (2017).** A neural network-based foF2 model for a single station in the polar cap. *Radio Science, 52*(6), 784–796. https://doi.org/10.1002/2016RS006192

**Bai, H., Feng, F., Wang, J., & Wu, T. (2020).** A combination prediction model of long-term ionospheric foF2 based on entropy weight method. *Entropy, 22*(4), 442. https://doi.org/10.3390/e22040442

**Basu, S., Groves, K., Basu, S., & Sultan, P. (2002).** Specification and forecasting of scintillations in communication/navigation links: Current status and future plans. *Journal of Atmospheric and Solar-Terrestrial Physics, 64*(16), 1745–1754. https://doi.org/10.1016/S1364-6826(02)00124-4

**Bello, S. A., Abdullah, M., Hamid, N. A., Reinisch, B., Yoshikawa, A., & Fujimoto, A. (2019).** Response of ionospheric profile parameters to equatorial electrojet over Peruvian station. *Earth and Space Science, 6*(4), 617–628. https://doi.org/10.1029/2018EA000537

**Bello, S. A., Abdullah, M., & Hamid, N. S. A. (2017a).** Investigation of ionospheric minimum frequency near dip equator. *Advanced Science Letters, 23*(2), 1329–1332. https://doi.org/10.1166/asl.2017.8357

**Bello, S. A., Abdullah, M., Hamid, N. S. A., & Reinisch, B. W. (2017b).** Comparison of ionospheric profile parameters with IRI-2012 model over Jicamarca. *Journal of Physics: Conference Series, 852*(012016). https://doi.org/10.1088/1742-6596/852/1/012016

**Bello, S. A., Abdullah, M., Hamid, N. S. A., Yoshikawa, A., & Olawepo, A. (2017c).** Variations of B0 and B1 with the solar quiet Sq-current system and comparison with IRI-2012 model at Ilorin. *Advances in Space Research, 60*(2), 307–316. https://doi.org/10.1016/j.asr.2017.02.003

**Bello, S. A., Abdullah, M., Hamid, N., Yusuf, K. A., Yoshikawa, A., & Fujimoto, A. (2023).** Robust least square modelling for selected daytime ionospheric parameters using geomagnetic observations at low latitudes. *Advances in Space Research, 72*(5), 1615-1633. https://doi.org/10.1016/j.asr.2023.04.040.

**Bello, S., Yusuf, K., Sharafa, S., Shehu, S., Joseph, O., & Oluwafemi, L. (2025).** DINData: A Windows Software to Reformat and Clean Digisonde Numeric Dataset. *BIMA Journal of Science and Technology Gombe, 9*(4A), 114–127. https://doi.org/10.64290/bima.v9i4A.1404

**Bi, C., Ren, P., Yin, T., Xiang, Z., & Zhang, Y. (2022).** Modeling and forecasting ionospheric foF2 variation in the low latitude region during low and high solar activity years. *Remote Sensing, 14*(21), 5418. https://doi.org/10.3390/rs14215418

**Bilitza, D., Altadill, D., Truhlik, V., Shubin, V., Galkin, I., Reinisch, B., & Huang, X. (2017).** International Reference Ionosphere 2016: From ionospheric climate to real-time weather predictions. *Space Weather, 15*(2), 418–429. https://doi.org/10.1002/2016SW001593

**Bilitza, D., Pezzopane, M., Truhlik, V., Altadill, D., Reinisch, B. W., & Pignalberi, A. (2022).** The international reference ionosphere model: A review and description of an ionospheric benchmark. *Reviews of Geophysics, 60*(4), e2022RG000792. https://doi.org/10.1029/2022RG000792

**Elseidi, M. (2024).** A hybrid Facebook Prophet-ARIMA framework for forecasting high-frequency temperature data. *Modeling Earth Systems and Environment, 10*(2), 1855–1867. https://doi.org/10.1007/s40808-023-01874-4

**Galkin, I., Reinisch, B. W., Huang, X., & Khmyrov, G. M. (2013).** Confidence score of ARTIST-5 ionogram autoscaling. *Ionosonde Network Advisory Group (INAG) Bulletin No, 73*, 1–7. https://www.ursi.org/files/CommissionWebsites/INAG/web-69/2008/artist5-inag.pdf

**Harvey, A. C., & Peters, S. (1990).** Estimation procedures for structural time series models. J*ournal of Forecasting, 9(2)*, 89–108. https://doi.org/10.1002/for.3980090203

**Huang, L., Wu, H., Lou, Y., Zhang, H., Liu, L., & Huang, L. (2022).** Spatiotemporal analysis of regional ionospheric TEC prediction using multi-factor NeuralProphet model under disturbed conditions. *Remote Sensing, 15*(1), 195. https://doi.org/10.3390/rs15010195

**Kelley, M. C. (2009).** The Earth's ionosphere. Academic Press (2nd ed., Vol. 96). International Geophysics Book Series.

**Kouris, S., & Nissopoulos, J. (1994).** Variation of foF2 with solar activity. *Advances in Space Research, 14*(12), 51–54. https://doi.org/10.1016/0273-1177(94)90238-0

**Liu, J. Y., Chen, Y. I., & Lin, J. S. (2003).** Statistical investigation of the saturation effect in the ionospheric foF2 versus sunspot, solar radio noise, and solar EUV radiation. *Journal of Geophysical Research: Space Physics, 108*. https://doi.org/10.1029/2001ja007543

**Oo, Z. Z., & Phyu, S. (2020).** Time series prediction based on Facebook prophet: A case study, temperature forecasting in myintkyina. *International Journal of Applied Mathematics Electronics and Computers, 8*(4), 263–267. https://doi.org/10.18100/ijamec.816894

**Reinisch, B., Huang, X., Galkin, I., Paznukhov, V., & Kozlov, A. (2005).** Recent advances in real-time analysis of ionograms and ionospheric drift measurements with digisondes. *Journal of Atmospheric and Solar-Terrestrial Physics, 67*(12), 1054–1062. https://doi.org/10.1016/j.jastp.2005.01.009

**Reinisch, B. W., & Galkin, I. A. (2011).** Global ionospheric radio observatory (GIRO). *Earth, Planets and Space, 63*(4), 377–381. https://doi.org/10.5047/eps.2011.03.001

**Tang, J., Li, Y., Yang, D., & Ding, M. (2022).** An approach for predicting global ionospheric TEC using machine learning. *Remote Sensing, 14*(7), 1585. https://doi.org/10.3390/rs14071585

**Tapping, K. F. (2013).** The 10.7 cm solar radio flux (F10. 7). *Space Weather, 11*(7), 394–406. https://doi.org/10.1002/swe.20064

**Taylor, S. J., & Letham, B. (2018).** Forecasting at scale. *The American Statistician, 72*(1), 37–45. https://doi.org/10.1080/00031305.2017.1380080

**Toharudin, T., Pontoh, R. S., Caraka, R. E., Zahroh, S., Lee, Y., & Chen, R. C. (2023).** Employing long short-term memory and Facebook prophet model in air temperature forecasting. *Communications in Statistics-Simulation and Computation, 52*(2), 279–290. https://doi.org/10.1080/03610918.2020.1854302

**Tsagouri, I., Koutroumbas, K., & Belehaki, A. (2009).** Ionospheric foF2 forecast over Europe based on an autoregressive modeling technique driven by solar wind parameters. *Radio Science, 44*(01), 1–21. https://doi.org/10.1029/2008RS004112

**Vishwas, B., & Patel, A. (2020).** Hands-on time series analysis with Python. Springer. https://doi.org/10.1007/978-1-4842-5992-4

**Wang, G. J., Shi, J. K., Wang, Z., Wang, X., Romanova, E., Ratovsky, K., & Polekh, N. M. (2017).** Solar cycle variation of ionospheric parameters over the low latitude station Hainan, China, during 2002–2012 and its comparison with IRI-2012 model. *Advances in Space Research, 60*(2), 381–395. https://doi.org/10.1016/j.asr.2016.12.013